Egypt. J. Chem. **Vol. 68**, No. 5 pp. 337 - 350 (2025)

Egyptian Journal of Chemistry

http://ejchem.journals.ekb.eg/

Enhancing Seismic Efficiency of Composite Steel Shear Walls Using Encased C-Shape Cold-Formed Steel

Mohamed Fekry [a]*, Sameh Gaawan[a], Mohamed Yehia [a]

[a]*Faculty of Engineering, Helwan Universityn Mataria, Cairo, 13113, Egypt*

Abstract

In order to improve the seismic behavior of reinforced concrete (RC) shear walls in high-rise structures, this research recommends employing an embedded cold-formed steel section (ECFS) composite wall. In order to determine how well composite shear walls withstand seismic activity, a battery of tests was run on four different specimens: two specimens with embedded CFS composite walls, one normal RC walls, and one cold formed steel bracing frame (CFSB-F). Specifically. A discussion was held regarding the experimental behavior of test specimens, covering topics such as load-deformation characteristics, damage development, energy dissipation, stiffness, failure mode, and ductility. As a result of the findings, it appears that composite shear walls that incorporate cold-formed steel have greatly improved lateral load can be reached over conventual wall by about 178 %, also Significantly enhancing stiffness of wall, and improvement in energy dissipation capacities by 16 %. Result showed good stability and performance of the composite shear wall with seismic loads in deformation capacity. Additionally, it was shown that crushing concrete could be reduced effectively. The maximum lateral load capacity was predicted using the Chinese Code for Design of Composite Structures. The comparison indicates a strong correlation between the test results and the estimated findings.

Keywords: Composite shear walls; Encased R-C walls; Quasi-static load; Cold-formed steel; skeleton curves.

1. Introduction

Over the past few years, a significant number of new skyscrapers have been built. Shear walls are typically the primary structural elements responsible for resisting lateral loads in these types of buildings. The magnitudes of the overall shear force escalate with the elevation of the structure. An increase in the thickness of the reinforced concrete (R.C) shear wall can lead to a decrease in its effective area and ability to deform, which in turn can negatively impact the seismic performance of the entire R.C structure. Researchers have enhanced the seismic performance and deformation capacity of the shear wall by using improvement strategies and conducting several investigations. Shear walls with concealed bracings are one example of these measures [1, 2].

Another method of reducing cracking is the use of steel-concrete composite shear walls. Composite shear walls have a lower cracking rate than RC shear walls, have a greater ductility and have a greater energy dissipation capacity than RC shear walls [3-5], the high rigidity and good overall performance of composite walls make them less susceptible to local buckling and lateral drift during earthquakes [6, 7]. Steel reinforced concrete shear walls [8], composite steel shear walls with an outer wrapping [9-12], composite shear walls with a concealed truss [13], and embedded composite steel plate-concrete shear walls [14, 15] are some of the subtypes of composite steel concrete shear walls. Integrating embedded steel sections with concrete results in the formation of composite shear walls, which are designed to make the most of the combination of steel and concrete.

Steel and concrete are able to carry vertical loads simultaneously as a result of this mechanism. Consequently, the shear wall can carry a greater load, has a smaller sectional size, and has a greater lateral stiffness, which can improve the structure's seismic performance overall. An experimental steel-concrete composite element is numerically analyzed and tested by Dan et al [16], Cho. [17], Qian et al [18], H. Omare [19].

Most noticeably different from one experimental element to the next is the configuration of the assembly of steel component inserted in the wall cross section and the encased element of the steel cross section. To secure the steel profiles to the concrete, several steel studs featuring heads are incorporated. Through the incorporation of steel tubing or section steel into the edge members, reinforced concrete shear walls can effectively augment their ductility, stiffness, and capacity to sustain loads. Recent research has led to the development of a new composite wall system that includes steel truss components integrated within it. This system incorporates web bracing diagonal members, which serve to enhance the wall's resistance to

*Corresponding author e-mail: engfekry89@gmail.com.; (Mohamed Fekry).
Received date: 14 August 2024, Revised date: 06 September 2024, Accepted date: 16 September 2024
DOI: 10.21608/ejchem.2024.312311.10193

shear stresses and its ability to dissipate energy [20- 22].

Further construction benefits can be obtained by incorporating cold-formed thin-walled (CFTW) steel sections into RC walls, thereby decreasing the quantity of reinforcing bars that are necessary. A CFTW steel sections can first be erected in both sides, and can be help to be sufficiently strong and stiff for all of the construction loads to be carried. The CFTW steel sections can be reinforced with reinforcement bars, while the formwork can be screwed with holes for the cover. Therefore, it is possible to reduce the amount of conventional formwork to a great extent [23, 24].

An analysis of the structural response of composite shear walls embedded with CFTW steel sections was examined in this study by examining the hysteretic responses, strength degradation characteristics and stiffness, failure pattern, ductility and energy dissipation capacity of the walls.

2. Experimental Program

2.1. Material Properties

Mixtures of concrete made for normal strength the concrete was made with a combination of natural sand for the fine aggregate, dolomite for the coarse aggregate, and 42.5 percent cement. It is produced by Helwan cement company in Egypt, Table 1 displays these mixtures.

Table 1: Proportioning of concrete mixes.

Cement (kg)	350
Sand (kg)	750
Gravel (kg)	1150
Water (liter)	180
Volume (m^3)	1

Concrete with an exacting specification of 30 MPa compressive strength was utilized in the construction of each test specimen. Upon the 28th day, the mean compressive strengths of the concrete measured in standard cubic sample tests of 150 mm by 150 mm by 150 mm were 28.89 MPa, 31.79 MPa, 35.88 MPa, and 33.1 MPa, respectively. Fig. 1 displays the preparation and testing of the compressive strength of the cubes.

Figure 1: Testing the compressive strength of the cubes

The coupon tests were performed on a universal testing machine; three coupons were tested for each material coil. According to the results of the coupon tests, the steel sheets that were utilized in this investigation conform the minimum standards for ductility. as shown in Fig. 2 Stress-strain of steel grade ST-37. The stress strain curve was constructed by using the average of the results of three different experiments performed in each group.

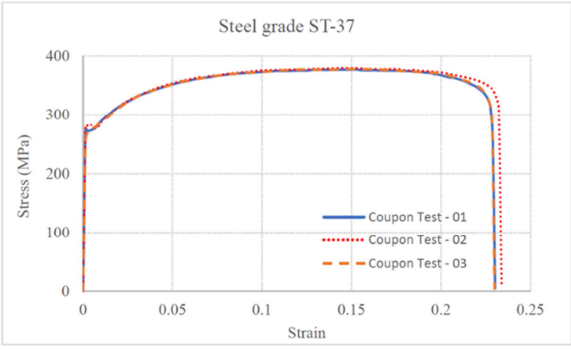

Figure 2: Stress-strain of steel grade ST-37

Table 2 displays the mechanical properties of the steel materials utilized for the tested walls, such as hot-rolled plain and ribbed steel bars for wall reinforcement, steel tube members, and cold-formed thin-walled sections.

Table 2: Properties of steel material

Type of steel	E_S (N/mm^2)	F_y (N/mm^2)	F_u (N/mm^2)
C80 * 58.5 * 1.5	2 * 10 5	378	424
Steel Tube	1.95 * 10 5	272	325
No. 8 HPB	2.08 *10 5	230	327
No. 10 HRB	2.11 * 10 5	504	565

2.2. Specimen Details

A total of four one-third scaled R.C. wall and composite shear walls, identified by Control Wall (C-W), Embedded Cold Formed Steel Bracing Wall (ECFSB-W), Embedded Cold Formed Steel Wall (ECFS-W), and Cold Formed Steel Frame (CFS-F), were erected and evaluated while subjected to both lateral loads and vertical load. It is important to note that all four specimens have identical overall dimensions, including a top loading block of 1100 mm * 250 mm * 250 mm, a wall portion of 1200 mm * 140 mm * 700 mm, and a base block of 1300 mm * 350 mm * 450 mm. We used eight hot-rolled plain bars (HRPs) of nominal diameter 8 mm and yield strength 240 MPa as horizontal reinforcement spaced 150 mm apart, and eight hot-rolled ribbed bars (HRBs) with a diameter 10 mm and yield strength 500 MPa as vertical reinforcement spaced 220 mm apart. The embedded section and web braces for specimen ECFSB-W were made of CFS C shape steel sections and steel tube with an internal diameter of 30mm and thickness of 2mm. The specimen ECFS-W contained vertical CFS C channel shapes of steel with dimensions of C80 * 58.5 * 1.5. Fig. 3 has a comprehensive description of the dimensions and characteristics of the shear wall, and the CFS-sectional dimensions encased in walls. Table 3 contains an overview of the main provided details and specifications for the four specimens. Fig. 4 displays the process of preparing a specimen and casting concrete.

Table 3: Specimen's details

Specimens	C-W	ECFS-W	ECFSB-W	CFSB-F
length x thickness x height	1200 mm x 700 mm x 140 mm			—
vertical wall reinforcement	8 @10	8 @10	8 @10	—
Horizontal wall reinforcement	7 @ 8/m	7 @ 8/m	7 @ 8/m	—
Steel form chord type	—	L 80-15	L 80-15	L 80-15
Steel form brace type	—	—	Tube bracing 2mm	Tube bracing 2mm
Axial ratio	0.1	0.1	0.1	0.1

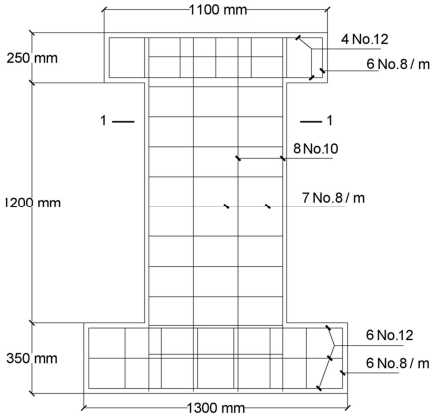

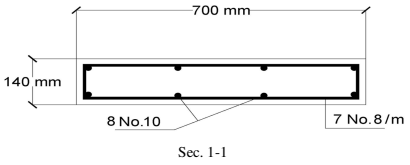

a) C-W Specimen

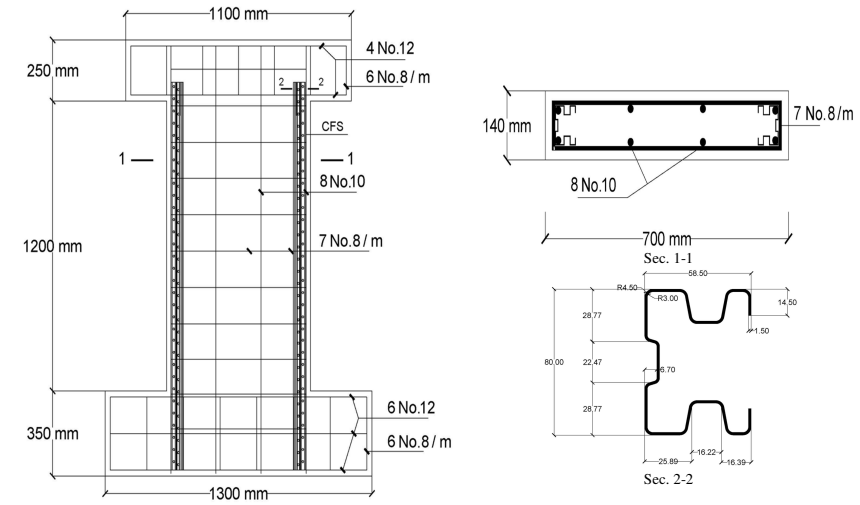

b) ECFS-W Specimen

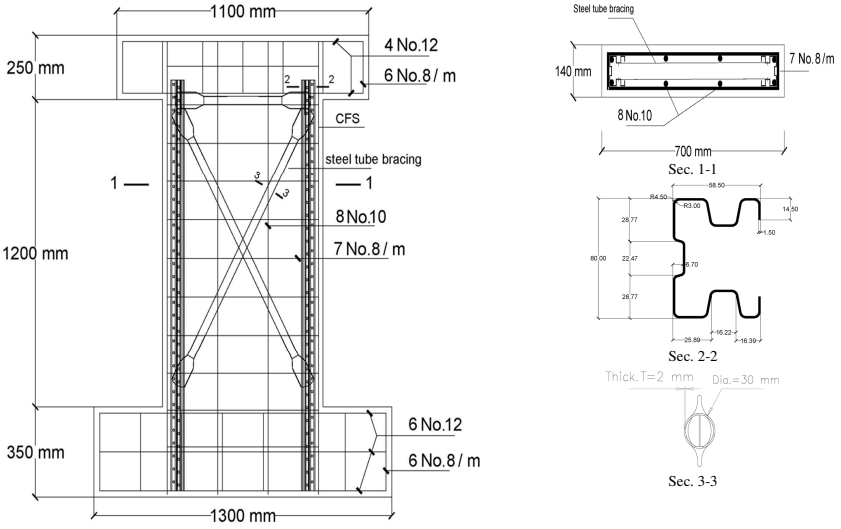

c) ECFSB-W Specimen

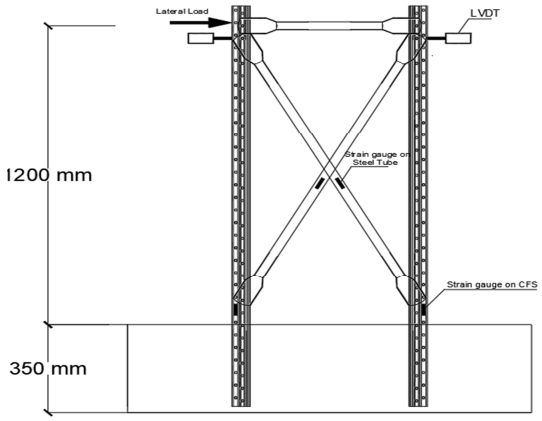

d) CFSB-F Specimen

Figure 3: Specifications of the examined samples

a) Preparing steel frame in cased frame works b) Casting Concrete

Figure 4: casting concrete and preparing specimen

2.3. Testing Setup

With the purpose of simulating earthquake conditions, three composite wall specimens were put through a series of tests that involved applying cyclic lateral load reversals and constant axial loads. The specimen was fastened to the sturdy frame using high-strength steel rods, as depicted in Fig. 5. In order to maintain a consistent axial force on the specimen, a hydraulic jack was used. The jack, which could support loads up to 1500 kN, was fastened to the frame girder using rods made of high-strength steel. Applying this force to the specimen was equivalent to applying the axial load ratio with a value of 0.1. As per the provided definition, the ratio of axial compression is determined by dividing the axial compression load exerted on the cross section by its overall capacity to bear axial loads. For details on the axial compressive applied load for each specimen, see Table 3. The top beam was equipped with two 100 mm stroke, horizontal hydraulic actuators that could withstand loads up to 1000 KN. Testing of all specimens was conducted under cyclically increasing horizontal loads, since the top beam was designed to transmit both constant vertical load and cyclic axial Hz forces. To prevent overturning and sliding during testing, in order to support the base block, a stiff beam was installed on both sides. The test was divided into two parts to make loading easier. The horizontal load was raised by 8 kN until it reached 24 kN at the start of the test. After that, the increase in the horizontal load dropped to 5 kN until the first crack in the concrete was seen going in the direction of the positive load. The loading pattern was then repeated in the opposite way until the first crack in the concrete showed up. We looked at the strength and stiffness degradation properties for each amount of displacement by doing two cycles. Testing was halted when either the axial load was insufficient to complete the task at hand or the lateral applied load capacity fell below 85% of its maximum Hz lateral load.

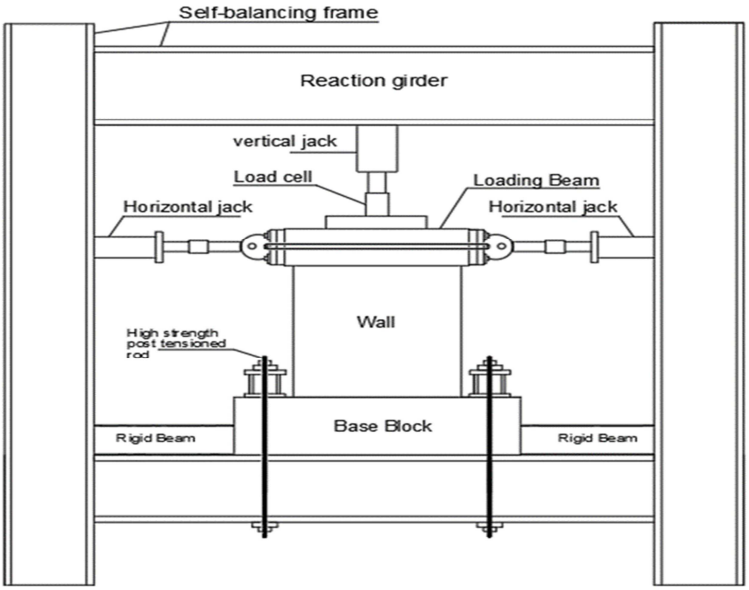

a) Detailed Graph for lab. setup

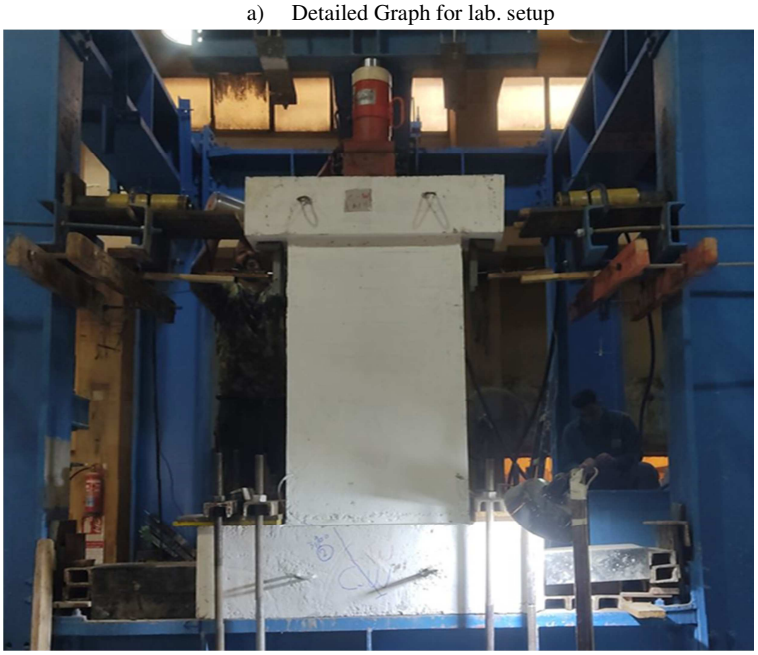

b) Lab. Setup

Figure 5: Specimens test setup

As shown in Fig. 6, adequate instrumentation was set up to test the specimens, Measure and document the applied force and change in deformation shape. Strain gauges were affixed at certain locations on reinforcement and embedded CFS members to quantify strain. Load cells and linear variable differential transformers (LVDTs) were placed atop the specimen in order to measure the lateral load and displacement. Additionally, experimental observations were documented, including the progression of fracture formation and the sequence of yielding.

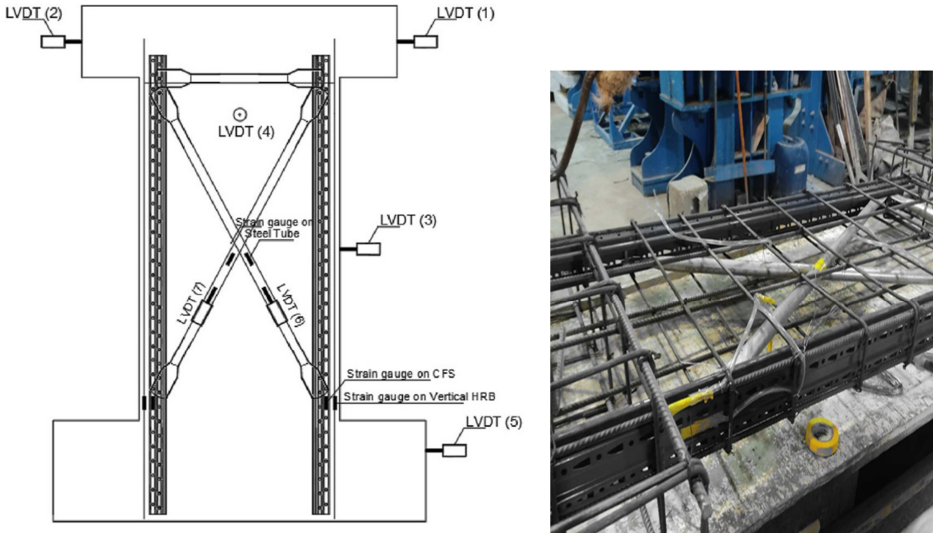

Figure 6: Installation details of the strain gauge and LVDT

3. Results and Discussion

3.1. General Observations

With a force of 39 kN, the specimen **C-W** was cracked. A number of inclined cracks emerged, each with a 1.35 mm lateral displacement. At 3.5 mm lateral displacement, the inclined cracks started to widen and horizontal cracks showed on the bottom wall. By the time 13.5 mm lateral displacement reached the boundary region, the wall's concrete had begun to crush. A maximum displacement of 15.2 mm was recorded during the loading cycles, when concrete spall off happened on the compression part at the bottom of the wall. The cracking load in specimen **ECFS-W** was 59 kN. The crack spread rapidly at a

displacement of 5.5 mm after cracking vertically at 1.2 mm on the compression side of the wall corner. A buckling formed on the longitudinal reinforcing bars, When the compressive side of the wall's concrete spalled off due to a 10 mm lateral displacement. The embedded CFS C-shaped steel member buckled at a displacement of 11.5 mm as well. Because the boundary elements were severely crushed by the concrete, the lateral load carrying capability of the ECFSW dropped dramatically at a 12 mm lateral displacement. The experimental phenomena observed during **ECFSB-W** were very similar to those observed during ECFSW. Cracking loads of 65 kN were observed for specimen ECFSBW. Conversely, tube bracing provided greater strength for specimen ECFSBW, which promptly buckled in response to a 13 mm lateral displacement, followed by the embedded CFS C-shaped truss chord buckling and longitudinal rebar fracture. Two factors contributed to the eventual collapse of **CFSB-F**: local buckling in the CFS C shape component and the bolted connection between the steel section and the tube bracing, which experienced an incredibly modest lateral force. Before and after the wall was subjected to severe lateral load, the cracking patterns of each specimen are depicted in Fig. 7.

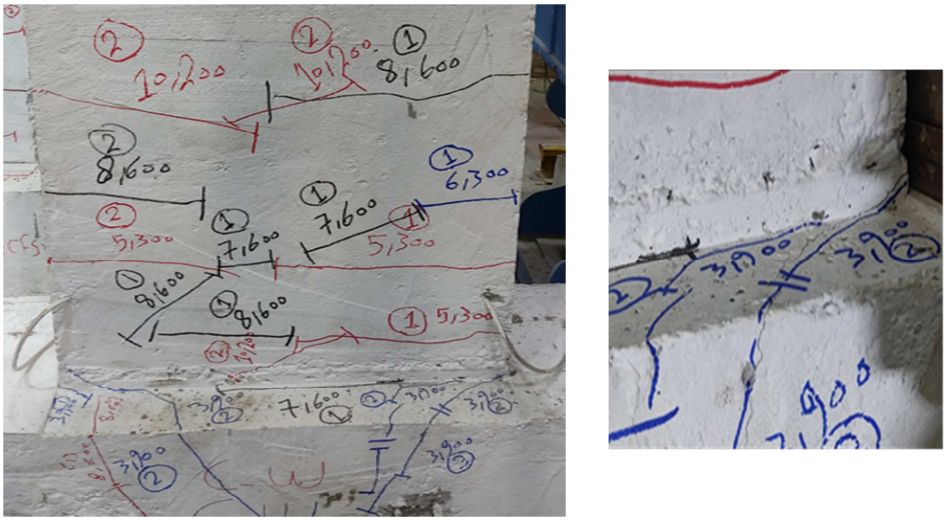

a) Failure pattern for C-W specimen

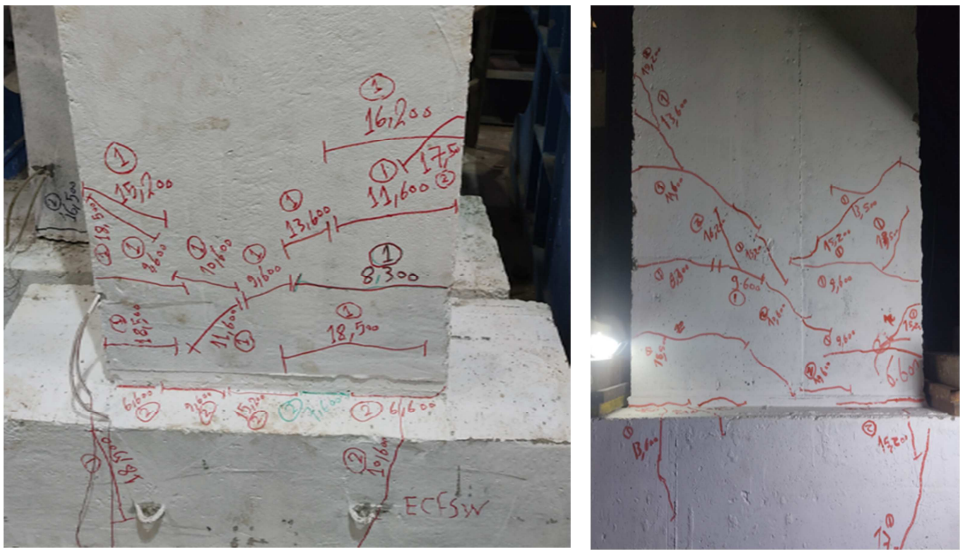

b) Failure pattern for ECFS-W specimen

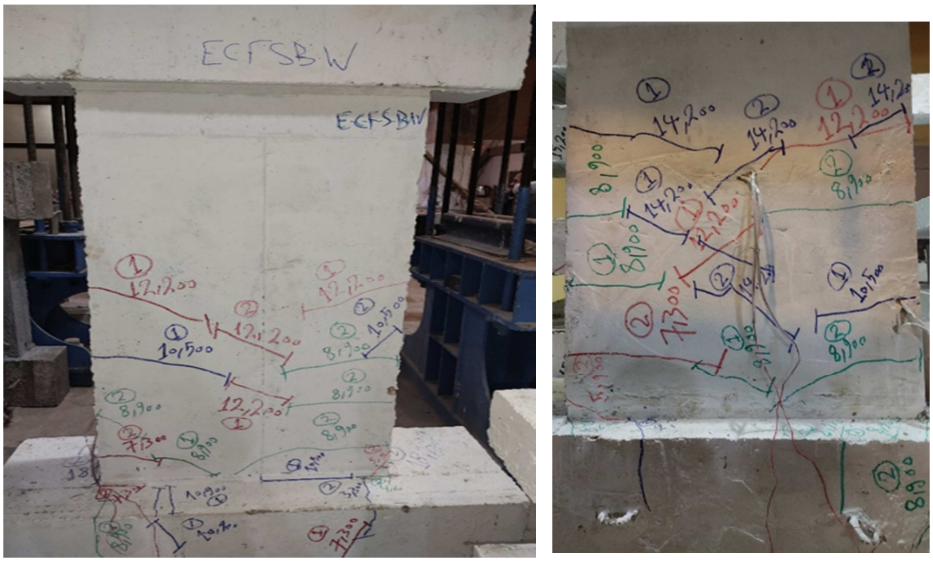

c) Failure pattern for ECFS-W specimen

Figure 7: Failure pattern of specimen

3.2. Hysteretic Cycles

Fig. 8a shown **C-W** specimen hysteresis loops involving shear force and lateral displacement. Hysteretic loops did not indicate obvious pinching during initial loading cycles. The specimen was yielded at a displacement of 3.36 mm after 97.5 kN of shear force was applied. In the both loading directions, the peak capacities to bear lateral loads were 118.6 kN, with corresponding displacements of approximately 14.7 mm. At a distance of 15.2 mm, the lateral load in two side of the wall decreased substantially and the surface concrete spalled off at the wall web. A relatively brittle failure pattern was observed for C-W, along with poor ductility and energy dissipation capability compared to other specimens.

As can be seen in Fig. 8b, the relationship between shear force and lateral displacement for **ECFS-W** is presented. In this case, the crack started widely with a displacement of 1.33 mm. This resulted in a lateral capacity of 78 kN as a result of the displacement. The maximum shear forces were measured to be 184.8 kN in both side for the loading position. As a result of the 9 mm lateral displacements, neither the lateral load nor the stiffness was affected in any way. The test was terminated because to the fact that the CFS was buckling and the boundary element concrete had a significant crushing, which resulted in a lateral displacement of 11.5 mm.

ECFSB-W exhibits a relationship between shear force and lateral displacement in Fig. 8c. The specimen demonstrates a linear correlation between lateral load and displacement up to a magnitude of 73 kN. The greatest lateral force measured in the positive loading direction was 198.5 kN, with a corresponding maximum displacement of 13.2 mm. In the negative loading direction, the maximum obtained load was 207.9 kN, with a lateral displacement of 11 mm. According to Fig. 8d, a specimen of **CFS-F** failed rapidly as a result of local buckling at a corresponding lateral load of 10 kN. CFS-F cannot resist lateral loads independently, but when enclosed in a R.C wall, it can enhance the overall resistance to lateral loads. Remarkably, the difference between ECFS-W and E CFSB-W is evident when compared to C-W.

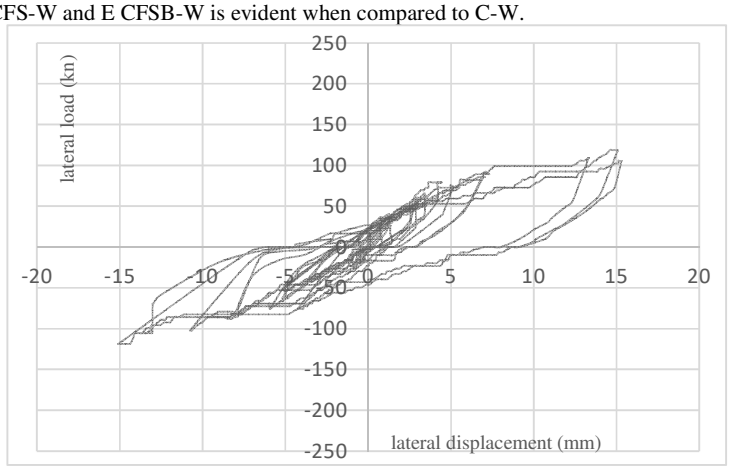

a) C-W

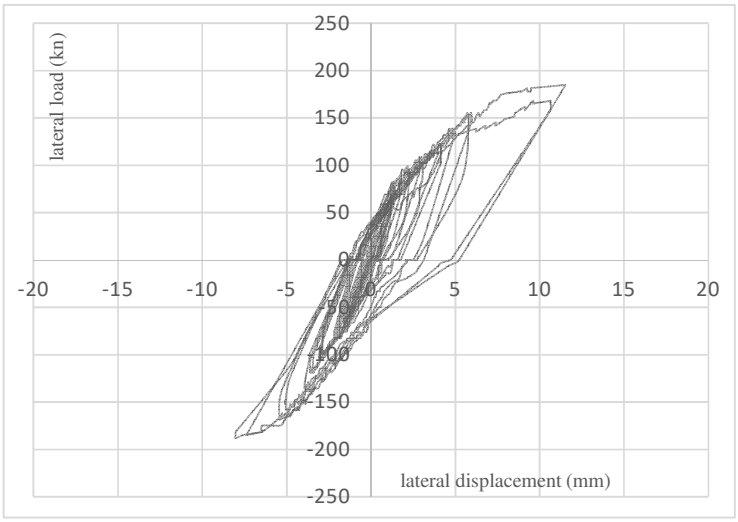

b) ECFS-W

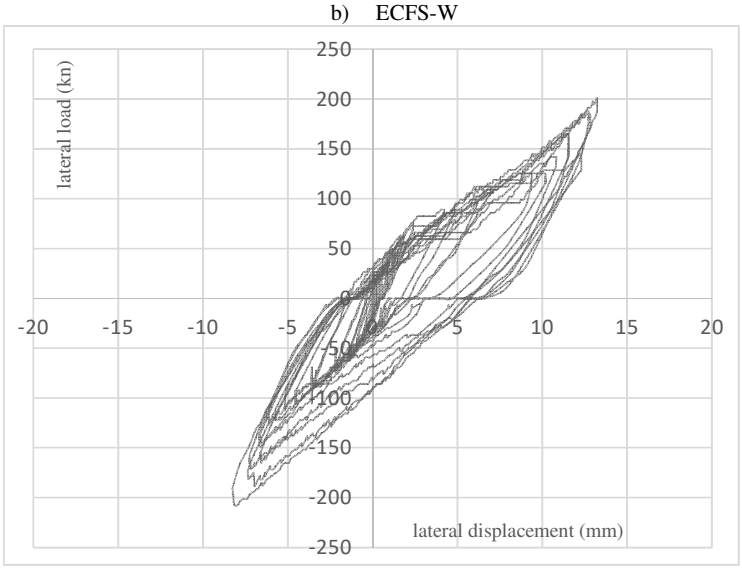

c) ECFSB-W

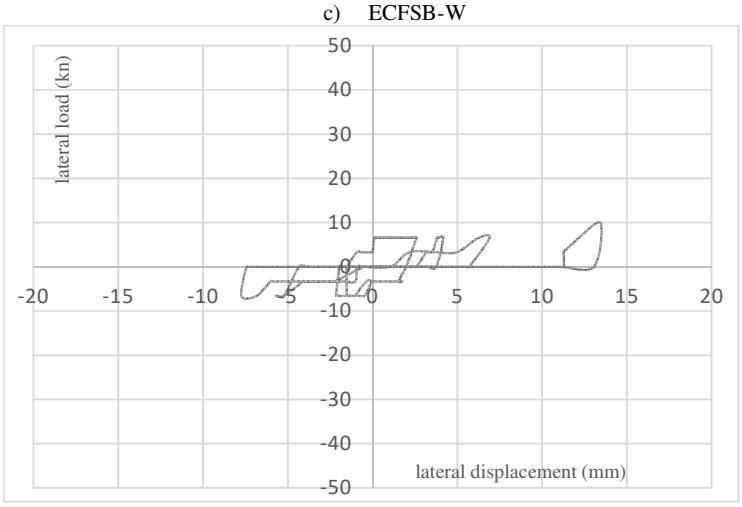

d) CFS-F

Figure 8: Specimen hysteresis loops for lateral load versus displacement relationships

3.3. Skeleton Curves

The skeleton curves illustrated in Fig. 9 represent the maximum loads applied to the test walls, in both directions, for each loading displacement, at the first cycle. According to the figure, shear walls exhibit ductile failure behavior during flexural failures, exhibiting minimal reduction in strength as displacement increases after reaching maximum load.

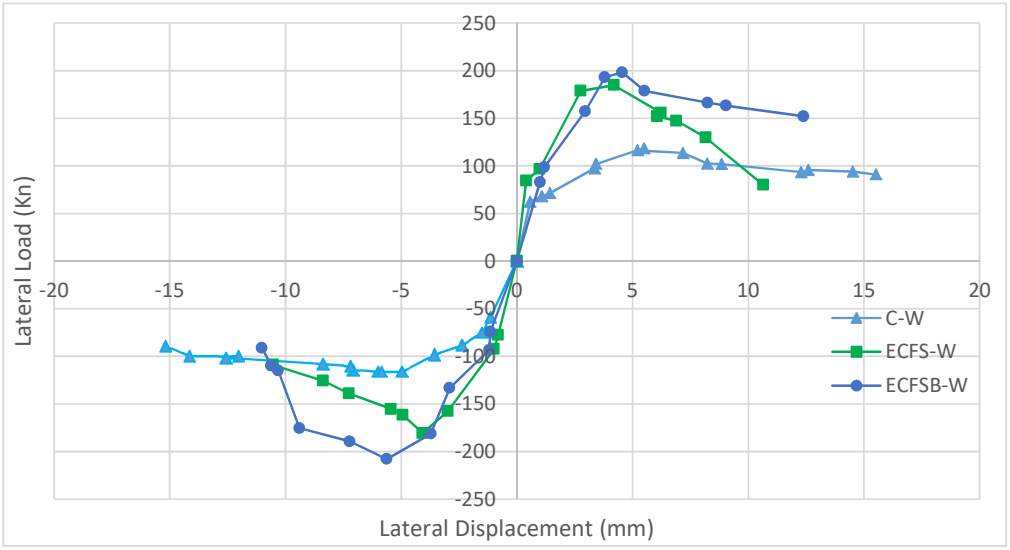

Figure 9: Test walls skeleton curves.

3.4. Ductility

The equivalent energy approach that was provided by Park [25] was utilized in order to determine the displacement ductility of each individual specimen. With the use of the following equation, the ductility of every specimen was determined by utilizing the ductility coefficient (μ).

$$\mu = \Delta_u/\Delta_y \quad (1)$$

where Δ_u horizontal displacement at the time of failure, and Δ_y at the yielding point. A summary of all specimens' ductility coefficients is provided in Table 4.

Table 4: Summary of all specimens' ductility coefficients

Specimen	Δ_y (mm)	Δ_u (mm)	Ductility μ
C-W	3.36	12.59	3.74
ECFS-W	2.36	6.06	2.56
ECFSB-W	3.79	7.51	1.98

A comparison of ECFS-W and ECFSB-W to C-W showed higher lateral load capacities, however, there was a greater reduction in ductility by 31 % and 49 %, respectively, when compared to C-W. It is important to note that the envelope curves of ECFS-W and ECFSB-W were nearly identical to one another, that exemplifies the high level of stability and performance of the encased shear wall with seismic loads.

3.5. Stiffness and Strength of Specimens

When cyclic loading was applied to embedded CF steel shear wall specimens, a Secant stiffness analysis was carried out in order to evaluate the stiffness degradation that occurred as a result of the loading. The Secant stiffness (Ki) of the composite wall specimens was determined by performing calculations using the provided equation.

$$Ki=P_i/\Delta_i \quad (2)$$

Where, P_i and Δ_i are the maximum lateral loads and displacement of the first i_{th} loading cycle.

Throughout the loading operation, the stiffness of all specimens dropped in accordance with a power law as the displacement of the specimens increased. Fig. 10 illustrates the correlation between stiffness and lateral displacement. The initial stiffness

of ECFS-W and ECFSB-W was larger than C-W. There was a very similar pattern for the degradation of stiffness in each specimen. C-W, however, demonstrated a much faster degradation of stiffness after significant strength degradation compared to other specimens, suggesting that tube bracing and embedded CFS have a beneficial effect. After loading all specimens except C-W, the stiffness degradation characteristics were very similar, demonstrating an insignificant effect of the tube bracing on stiffness degradation characteristics during the entire loading procedure.

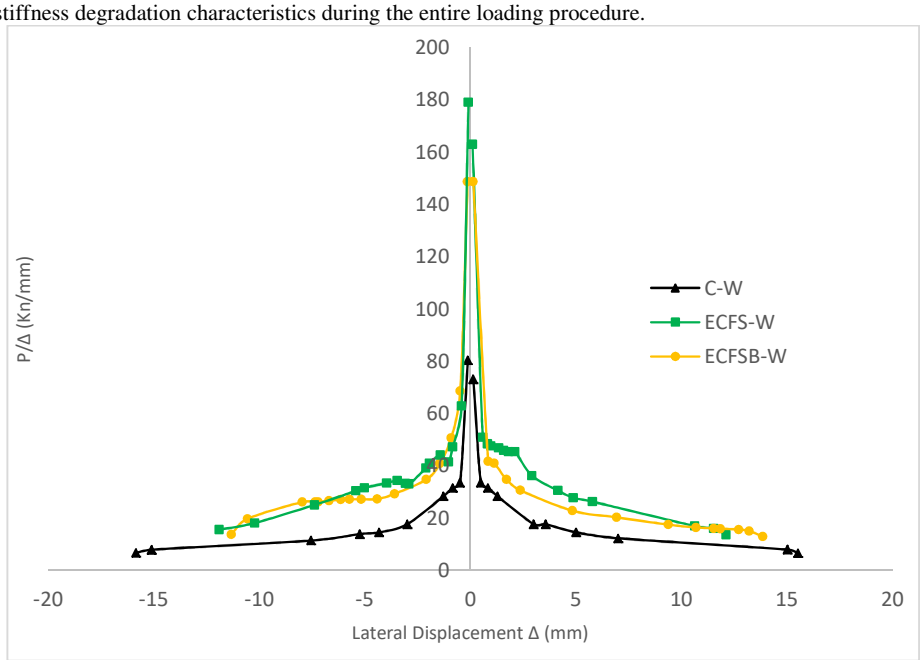

Figure 10: changes in the rate of stiffness deterioration in experimental walls

3.6. Dissipated Energy

Dissipation of energy through hysteretic damping (Wd) is a crucial factor in evaluating the seismic performance of a shear wall as it plays a significant role in reducing earthquake damages and minimizing the strength and ductility requirements of the structure in seismic design. Based on the area enclosed by the hysteresis loop at each loading increment, the dissipated energy can be calculated [26], as shown in Fig. 11.

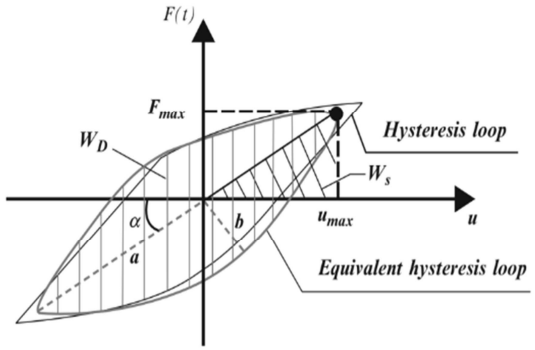

Figure 11: Energy dissipated from an equal-amplitude hysteresis loop [26]

A shear wall's energy dissipation capacity can be assessed by measuring its equivalent viscous damping ratio (εeq). According to [26], it is defined as follows:

$$\varepsilon_{eq} = \frac{W_D}{4*\pi*W_S} \quad (3)$$

As shown in Fig. 9, WD represents the dissipated energy, while WS represents the elastic strain energy that can be calculated by using the trilateral area (the vertically hatched area).

This Fig. 12 presents the number of cycles in which the specimens dissipated energy during the loading cycle. The wall demonstrated a favorable energy dissipation capacity based on the observation that all specimens showed a significant increase in dissipated energy as the loading displacement increased consecutively. In comparison with the other specimens,

the ECFSB-W exhibited the most advantageous energy dissipation capacity due to tube bracing and the concentration of steel channel members at the sides. The energy dissipation capacities of specimens ECFS-W and ECFSB-W were increased by 14 %, and 16%, respectively, as compared with specimen C-W. There is no doubt that tube bracing and CFS can effectively enhance shear wall energy dissipation.

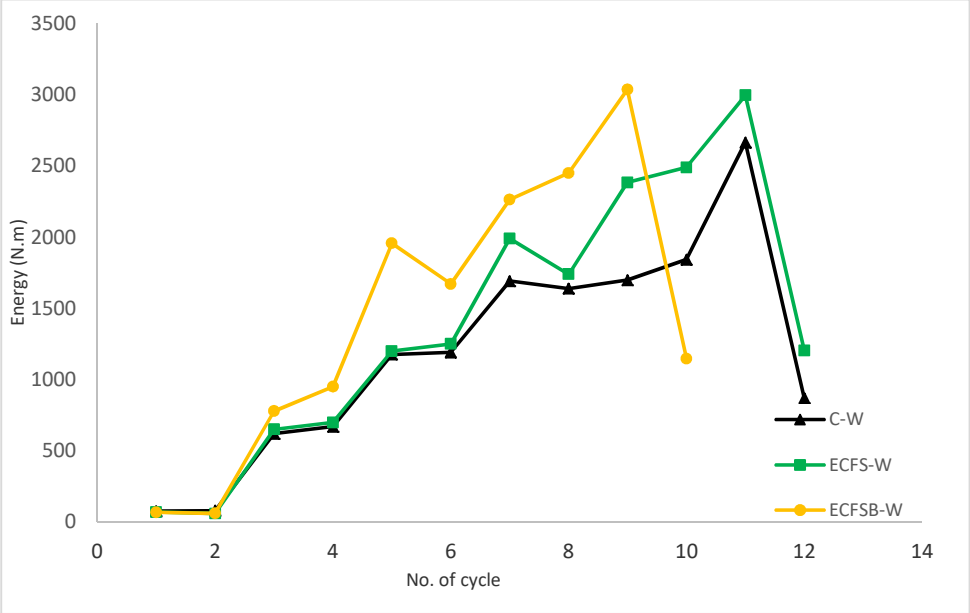

Figure 12: dissipated energy and number of cycles

4. Shear Strength Evaluation

Shear strength of reinforced concrete walls with CFS trusses embedded therein were examined in this research according to the Chinese Code for Design of Composite Structures JGJ 138-2016 [27]. This composite wall's shear strength is estimated to be affected by five factors: the concrete's shear strength, the axial load, the horizontally distributed reinforcement, the encased steel channel, and the encased steel bracing. With the following equation,

$$V_n = V_{RC} + V_{SC} + V_{SB} \quad (4)$$

$$V_{RC} = (1/(\lambda - 0.5))\,(0.4 * f_t * b_w * h_{w0} + 0.1 * N * (A_w/A) + 0.8 * f_{yh} * (A_{sh}/S) * h_{w0} \quad (5)$$

$$V_{SC} = (0.32/A) * f_a * A_a \quad (6)$$

$$V_{SB} = \left(f_g * A_g + \varphi * f'_g * A'_g\right) * cos(\theta) \quad (7)$$

Where V_n is the total lateral shear force in shear wall, V_{RC}, V_{SC}, and V_{SB} represent shear force from concrete, embedded CFS, and encased steel bracing respectively, λ The shear span ratio of a wall is limited to 1.5 to 2.2 and taken in this study equal 2.2, f_t=0.395 * $f_c^{0.55}$, b_w the thickness of wall, h_{w0} depth of effective shear, N is the axial load, which may be determined using the formula N=0.2*f_c*b_w*h_{w0} , A area of the wall's total cross-section, A_W the cross section area of the web, f_{yh} is the horizontal reinforcing bars' yield strength., A_{sh} It represents the the entire surface area of the horizontal reinforcing at a distance of S, where S stands for the distance between the horizontal reinforcing bars, A_a is the cross section area of encased CF steel section in the wall boundary of one side, f_a represents the yield strength of a CF steel section that is encased., A_g, A_g' are tensile and compressive area of steel tube diagonal bracing, θ is the angle of diagonal member and taken in range sixty degree for all specimen, and φ denotes the stability coefficient of the web brace under compression and take for bracing equal 0.537. This value is determined by the Chinese code for design of steel structures (GB500017-2003). The value for each specimen is presented in Table 5.

Table 5: Shear strength calculations and their components

Specimen	V_{test} (Kn)	JGJ 138-2016				V_{test}/V_n
		V_{RC} (Kn)	V_{SC} (Kn)	V_{SB} (Kn)	V_n (Kn)	
C-W	118.6	119.5	—	—	119.52	0.99
ECFS-W	184.8	119.5	25.04	—	144.56	1.26
ECFSB-W	207.9	119.5	25.04	72.70	217.27	0.96

There is a striking agreement between the tested wall and the numerical calculation with respect to the maximum lateral load, as shown in Fig. 13.

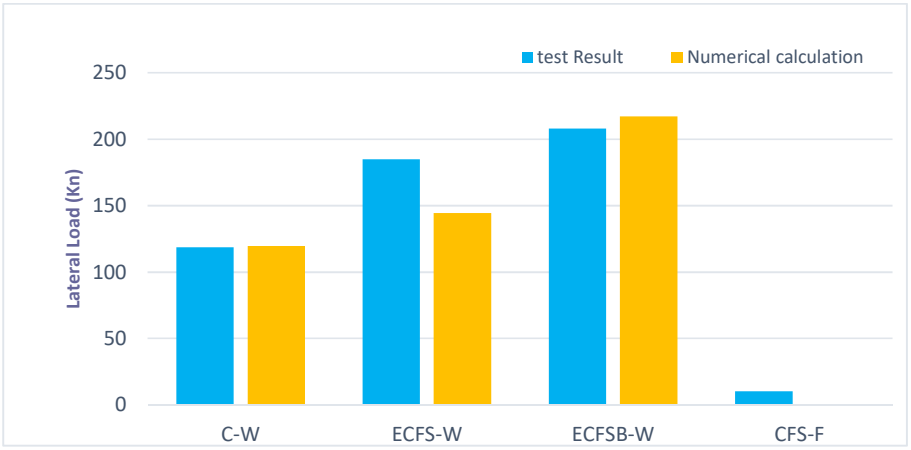

Figure 13: relation between tested wall and numerical calculation

5. Conclusion

This research program is aimed at proposing and studying shear walls embedded with CF steel members, Shear walls that are specifically designed for high-rise buildings in earthquake-prone zones are more suitable than traditional shear walls. four specimens were tested to evaluate seismic performance Based on their maximum lateral load capacity, energy dissipation capabilities, post-yielding deformation, and strength and stiffness degradation characteristics, based on the data and results, the following conclusions can be discussion.

- ECFS-W and ECFSB-W demonstrated 160% and 178% higher lateral load capacities compared to C-W, but also exhibited a 31% and 49% reduction in ductility, respectively. The stiffness analysis indicated superior stability and performance of the composite shear for specimens ECFS-W and ECFSB-W under seismic loads in comparison to C-W. Specimens ECFS-W and ECFSB-W showed a 14% and 16% improvement in energy dissipation capacities compared to specimen C-W.
- The experimental results show that the shear walls crushing failure pattern may be effectively changed by using embedded CF steel and tube braces. A favored failure pattern was noted in specimens that had embedded CF steel and tube bracing. Tube Bracing may help improve the deformation capacity, ductility, and energy dissipation of RC composite shear walls, according to a hysteretic response of the specimens.
- Steel tube bracing increases the amount of lateral forces applied to the wall web area. The wall web area must withstand these stresses, leading to the formation of additional inclined cracks in the wall web. The experiments on ECFS-W and ECFSB-W showed a big similarity in results, indicating that increasing the volumetric steel ratio for tube bracing will not significantly change the lateral load capacity and failure patterns of the wall.
- It is possible to accurately predict the maximum lateral load capacity of composite walls with encased CF steel using the calculation method provided in the Chinese Code for Design of Composite Structures (JGJ138-2016 2016).

6. Conflicts of Interest

The writers affirm that they do not have any conflicting interests.

7. Acknowledgments

The authors would express gratitude to the lab staff members of Materia and Cairo university to provide us with the correct equipment needed to fulfill this research.

8. Reference

[1] M. Zhang, J. Zhang, Y. Sun, and H. Dong, "Enhancing Seismic and Resilient Performance of Resilient Walls with Concealed Bracings: Experimental and Numerical Investigation," 2024, doi: 10.21203/rs.3.rs-4584875/v1.
[2] W. Cao, J. Zhang, J. Zhang, and M. Wang, "Experimental study on seismic behavior of mid-rise RC shear wall with concealed truss," *Front. Archit. Civ. Eng. China*, vol. 3, no. 4, pp. 370–377, 2009, doi: 10.1007/s11709-009-0062-x.
[3] H. Wu, T. Tu, L. Sui, F. Yan, and T. Zhou, "A novel modular CFS composite frame-wall structure: Experimental investigation and numerical analysis," *J. Constr. Steel Res.*, vol. 218, p. 108702, 2024, doi: 10.1016/j.jcsr.2024.108702.
[4] Y. Yu, Q. Xie, Y. Liu, and Y. Xue, "Cyclic Behavior of Partially Prefabricated Steel Shape-Reinforced Concrete Composite Shear Walls: Experiments and Finite Element Analysis," *Buildings*, vol. 14, no. 7, p. 2208, 2024, doi: 10.3390/buildings14072208.
[5] Q. Zhao and A. Astaneh-Asl, "Cyclic Behavior of Traditional and Innovative Composite Shear Walls," *J. Struct. Eng.*, vol. 130, no. 2, pp. 271–284, 2004, doi: 10.1061/(asce)0733-9445(2004)130:2(271).
[6] X. Ji, S. Zhang, X. Cheng, X. Jia, and M. Xu, "Cyclic In-Plane Shear Behavior of Composite Plate Shear Walls-Concrete Encased," *J. Struct. Eng.*, vol. 149, no. 11, p. 4023146, 2023, doi: 10.1061/jsendh.steng-11803.
[7] R. A. Link and A. E. Elwi, "Composite concrete-steel plate walls: analysis and behavior," *J. Struct. Eng.*, vol. 121, no. 2, pp. 260–271, 1995.
[8] Y. Hu, J. Zhao, D. Zhang, and Y. Li, "Cyclic performance of concrete-filled double-skin steel tube frames strengthened with beam-only-connected composite steel plate shear walls," *J. Build. Eng.*, vol. 31, p. 101376, 2020, doi: 10.1016/j.jobe.2020.101376.
[9] X. Gao, Z. Xu, X. Ren, and J. Li, "Experimental analysis of RC and SPRC squat shear walls," *J. Build. Eng.*, vol. 93, p. 109861, 2024, doi: 10.1016/j.jobe.2024.109861.
[10] J. G. Nie, H. S. Hu, J. S. Fan, M. X. Tao, S. Y. Li, and F. J. Liu, "Experimental study on seismic behavior of high-strength concrete filled double-steel-plate composite walls," *J. Constr. Steel Res.*, vol. 88, pp. 206–219, 2013, doi: 10.1016/j.jcsr.2013.05.001.
[11] H. S. Hu, J. G. Nie, J. S. Fan, M. X. Tao, Y. H. Wang, and S. Y. Li, "Seismic behavior of CFST-enhanced steel plate-reinforced concrete shear walls," *J. Constr. Steel Res.*, vol. 119, pp. 176–189, 2016, doi: 10.1016/j.jcsr.2015.12.010.
[12] J. J. Wang, X. Nie, F. M. Bu, M. X. Tao, and J. S. Fan, "Experimental study and design method of shear-dominated composite plate shear walls," *Eng. Struct.*, vol. 215, p. 110656, 2020, doi: 10.1016/j.engstruct.2020.110656.
[13] W. L. Cao, J. W. Zhang, J. P. Tao, and M. Wang, "Experimental study on low-rise RC shear wall with concealed truss," *J. southeast Univ.*, vol. 37, no. 2, pp. 195–200, 2007.
[14] W. Wang, Y. Wang, and Z. Lu, "Experimental study on seismic behavior of steel plate reinforced concrete composite shear wall," *Eng. Struct.*, vol. 160, pp. 281–292, 2018, doi: 10.1016/j.engstruct.2018.01.050.
[15] M. Meghdadian, N. Gharaei-Moghaddam, A. Arabshahi, N. Mahdavi, and M. Ghalehnovi, "Proposition of an equivalent reduced thickness for composite steel plate shear walls containing an opening," *J. Constr. Steel Res.*, vol. 168, p. 105985, 2020, doi: 10.1016/j.jcsr.2020.105985.
[16] D. Dan, A. Fabian, and V. Stoian, "Theoretical and experimental study on composite steelconcrete shear walls with vertical steel encased profiles," *J. Constr. Steel Res.*, vol. 67, no. 5, pp. 800–813, 2011, doi: 10.1016/j.jcsr.2010.12.013.
[17] S. H. Cho, B. Tupper, W. D. Cook, and D. Mitchell, "Structural Steel Boundary Elements for Ductile Concrete Walls," *J. Struct. Eng.*, vol. 130, no. 5, pp. 762–768, 2004, doi: 10.1061/(asce)0733-9445(2004)130:5(762).
[18] J. Qian, Z. Jiang, and X. Ji, "Behavior of steel tube-reinforced concrete composite walls subjected to high axial force and cyclic loading," *Eng. Struct.*, vol. 36, pp. 173–184, 2012, doi: 10.1016/j.engstruct.2011.10.026.
[19] H. Omare, "Tube Composite Shear Walls Abstract :," no. February 2022, 2023.
[20] Y. Xing, W. Wang, Y. Ou, X. Jiang, and H. Al-azzani, "Seismic behavior of steel truss and concrete composite shear wall with double X-shaped braces," *J. Build. Eng.*, vol. 62, p. 105399, 2022, doi: 10.1016/j.jobe.2022.105399.
[21] X. Ji, T. Leong, J. Qian, W. Qi, and W. Yang, "Cyclic shear behavior of composite walls with encased steel braces," *Eng. Struct.*, vol. 127, pp. 117–128, 2016, doi: 10.1016/j.engstruct.2016.08.041.
[22] W. Lan, B. Li, and Z. Zhang, "Seismic performance of steel-concrete composite structural walls with prestressed internal bracing," *J. Constr. Steel Res.*, vol. 140, pp. 11–24, 2018, doi: 10.1016/j.jcsr.2017.10.019.
[23] W. Qiao, X. Zhang, Q. Xu, and G. Wang, "Seismic performance of thin-walled steel and concrete composite column-corrugated steel shear wall structure," *J. Constr. Steel Res.*, vol. 201, p. 107745, 2023, doi: 10.1016/j.jcsr.2022.107745.
[24] Y. Wu, J. Zhang, Y. bin Yang, P. Ye, and Y. Xiao, "Seismic performance of reinforced concrete squat walls with embedded cold-formed and thin walled steel truss," *Eng. Struct.*, vol. 132, pp. 714–732, 2017, doi: 10.1016/j.engstruct.2016.11.061.
[25] R. Park, "Ductility evaluation from laboratory and analytical testing," in *Proceedings of the 9th world conference on earthquake engineering*, Tokyo-Kyoto Japan, 1988, pp. 605–616.
[26] G. P. Cimellaro and S. Marasco, *Introduction to dynamics of structures and earthquake engineering*, vol. 45. Springer, 2018.
[27] "JGJ 138-2016," in *Code for Design of Composite Structures*, China: China Architecture & Building Press, 2016.